A Numerical Investigation on the Ballistic Performance of Ceramic Composite Armors against EFP Threats

M. Emin Akca[1], M. Bartu Ünal[2], Koray Kaya[3], H. Hüseyin Türkmen[4]

[1]Nurol Teknoloji - R&D Analysis and Simulation, emin.akca@nurolteknoloji.com

[2]Nurol Teknoloji - R&D Analysis and Simulation, bartu.unal@nurolteknoloji.com

[3]Nurol Teknoloji - R&D Analysis and Simulation, koray.kaya@nurolteknoloji.com

[4]Nurol Teknoloji - R&D Advanced/Technical Materials, huseyin.turkmen@nurolteknoloji.com

1   Abstract

The increasing destructiveness of explosive-formed penetrators or projectiles (EFPs) in modern warfare has posed significant challenges in developing effective armored solutions incorporating advanced ceramics as crucial components, offering enhanced protection against high-velocity-formed projectiles. [1] In other words, Explosively Formed Penetrators pose a significant threat to military vehicles, necessitating the development of advanced armor solutions to counteract their destructive potential. Thus, Finite Element Analysis (FEA) research is crucial for the armor system against this threat. In addition, since EFP tests are costly and time-demanding, performing these experiments with FEA provides significant cost and performance efficiency. This study analyzes the composite armor system integrating Nurol Teknoloji [2] ceramics against EFP threats utilizing LS-DYNA, a program for nonlinear dynamic analysis of structures in three dimensions. [3]

2   Introduction

In recent years, the increasing threat of modern asymmetric warfare and the proliferation of advanced munitions have led to significant advancements in the design and development of protective armor systems. One of the critical challenges armor designers face is the need to mitigate the destructive effects of Explosively Formed Projectiles (EFPs). [4] These types of projectiles are characterized by their ability to penetrate even the most resilient armor materials due to their unique slug-forming mechanisms. Consequently, there continues to be a critical demand for innovative armor solutions to effectively counter EFP threats while maintaining a reasonable balance between weight, performance, and cost.

Wang et al. [5] experimentally investigated the effects of liner material, liner thickness, cone angle, and standoff distance on the penetration performance of the EFP into a 48 MPa normal strength concrete (NSC) target. These studies demonstrated that the EFP with a copper liner induced a greater penetration depth but a smaller borehole diameter than those with aluminum liners. Additionally, it was observed that as the EFP impact velocity increased, the penetration depth and borehole diameter increased and decreased quadratically, respectively.

EFPs are primarily used to defeat metal armor or ceramic/metal composite targets, such as tanks and ships. Therefore, the impact performance of EFPs on metal targets is often of more significant concern to weapon and armor designers. In this context, Yang et al. [6] investigated the interactions of EFPs with metals and examined the ballistic performance interactions with different thicknesses of EFP liners.

Ceramic composite materials have emerged as promising candidates for enhancing armor performance against various ballistic threats, including EFPs. These composites have a combination of high hardness, durability, and lightweight properties, making them particularly attractive for armor applications. Additionally, their ability to fracture and absorb energy upon impact can significantly contribute to the disruption of EFP penetrators, thereby increasing the probability of preventing complete penetration through the armor system.

This study aims to comprehensively examine the ballistic performance of a ceramic composite armor system against EFP threats. Through advanced numerical simulations, the interaction mechanisms between EFP penetrators and ceramic composite armor are aimed to be deeply understood. The results of this research are expected to provide insights into the effectiveness of ceramic composite materials as a method for safeguarding personnel and critical assets against EFP-induced damage. In addition, another impact analysis of EFP on armor steel is conducted to compare the ceramic composite armor produced by Nurol Teknoloji and the armor steel having the same weight with the same area.

3   Methodology

Both Lagrangian and Eulerian elements are utilized to analyze EFP impacts on targets. The ceramic composite armor, steel armor, and casing of the EFP are modeled via Lagrangian elements; however, since the deformation of high explosive (HE) and shaped liner are much larger, the Lagrangian description of motion is not applicable for the element distortions of those parts. Thus, the Eulerian mesh is generated for those materials. As a result, the Arbitrary Lagrangian-Eulerian (ALE) methodology with Fluid-Structure Interaction (FSI) algorithm is necessary for finite element analysis of EFP threats. [7]

In this study, a Lagrangian mesh of armors and the casing of EFP is formed by using 3D solid elements as usual. In the ALE methodology, the Eulerian domain is generally modeled via 3D solid elements, which seriously increases the number of elements and nodes when the mesh structure is a simple rectangular box with rectilinear elements. In addition, this high number of elements and nodes slows down the pre-processing of the model. To overcome these problems, LS-DYNA provides a method called Structured ALE (S-ALE), which aims to solve ALE problems involving rectilinear mesh and runs the analysis faster and more stable with less memory. [8]

The Eulerian domain comprises the air between EFP and the target, high explosives, shaped liner, and vacuum environment. These four materials lie within the Eulerian domain, necessitating the use of `*ALE_MULTI-MATERIAL_GROUP` (AMMG). Then, the structured (rectilinear) mesh and the S-ALE parts are formed, as indicated in Hao Chen's tutorial. [9] `*ALE_STRUCTURED_MESH` forms the domain to provide room for the fluids to occupy and flow, `*ALE_STRUCTURED_MESH_CONTROL_ POINTS` determines the boundaries of the ALE domain, and lastly `*ALE_STRUCTURED_ MESH_VOLUME_FILLING` explicitly fulfills the high explosive and shaped liner shells with the corresponding AMMGs within the ALE mesh. Lastly, `*ALE_STRUCTURED_MESH_TRIM` is used to improve efficiency and reduce computation time by trimming the structured mesh's unnecessary regions.

For the contact mechanisms between the Lagrangian parts of the target, four contact keywords are utilized: `CONTACT_AUTOMATIC_SURFACE_TO_SURFACE` is used between rigid clamps and the multi-layer composite armor parts, `CONTACT_AUTOMATIC_ONE_WAY_SURFACE_TO_SURFACE_TIEBREAK` is used between the layers of first composite part and also to model the adhesion between composite part and other materials, `CONTACT_AUTOMATIC_SURFACE_TO_SURFACE_TIEBREAK` is used between the layers of UHMWPE, and lastly, a generic `CONTACT_ERODING_SINGLE_SURFACE` is used to account for element erosion on contact surfaces.

Since there are both Lagrangian and Eulerian elements, a penalty-based Fluid-Structure Coupling algorithm is necessary to capture the interaction between them in which the total energy of the system is preserved as well as possible. For this purpose, LS-DYNA has two alternative keywords: `*STRUCTURED_FSI` and `*CONSTRAINED_LAGRANGE_IN_SOLID`. By trial and error, although it is much easier to use and faster, it has been observed that `*STRUCTURED_FSI` may not capture the Lagrangian-Eulerian coupling in EFP impacts with high velocities. Therefore, `*CONSTRAINED_ LAGRANGE_IN_SOLID` is used between the S-ALE part, casing, and target. A penalty coupling that allows element erosion in Lagrangian entities is applied in the normal direction, tension, and compression.

To achieve a better energy balance, hourglass, sliding interfaces, damping, material energies, and dissipated kinetic and internal energies are computed in the analysis. Improved advection logic is utilized, and ALE mesh smoothing is turned off. To initiate the explosion, `*INITIAL_DETONATION` is defined on the S-ALE part. The detonation point is chosen at a coordinate lying within the steel casing and on the top center of the high explosive material.

4   Numerical Modeling

4.1   FEM Parts
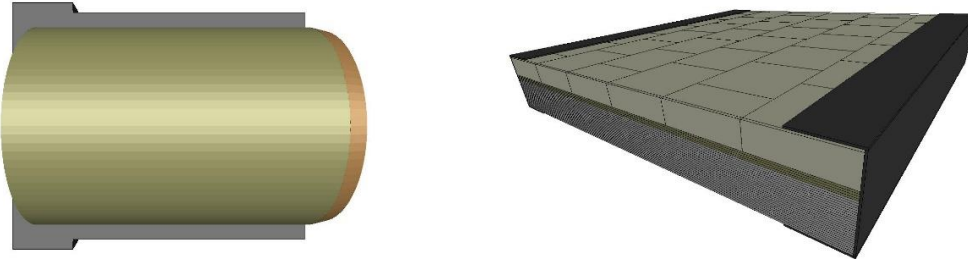
Fig.1:   Numerical model of (a) casing, high explosive, liner, and (b) clamped ceramic composite armor

The geometry of the FEM parts is represented in Fig. 1. Note that only the half-section of the casing is shown for simplicity. The interior region of the casing is filled with high explosive material, and the shaped liner is just placed in front of the HE. The composite armor panel is fixed in all directions and rotations by rigid clamps from two sides. Ceramic tiles are placed within a thin layer –*transparent in the figure*- and a thick layer of composite materials. Ultra-high molecular weight polyethylene (UHMWPE) polymer material is placed at the backmost of the armor.

Except for HE and the shaped liner, all the parts in the numerical model are modeled with 3D solid elements. HE and liner are meshed with shell elements since their volumes will be filled by S-ALE elements in the solution of the analysis. The whole model, including all the Lagrangian parts and the S-ALE multi-material mesh, is shown in Fig. 2.
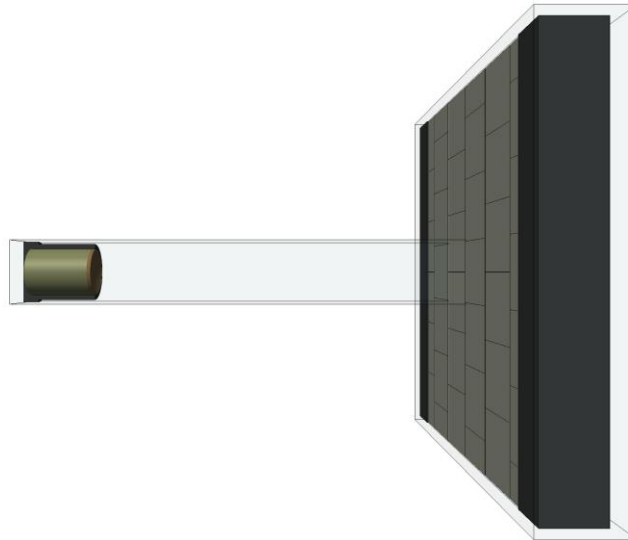
Fig.2:   3D model of EFP and composite armor together with S-ALE multi-material group domain

The number of elements for each part is represented in *Table 1.* The total number of the Lagrangian and S-ALE elements in the model equals 2,134,056 and 6,653,500, respectively.

FEM Part	Element type	Number of the elements
Casing	Hexahedral solid	33,600
High explosive	4-node shell	7,488
Shaped liner	4-node shell	3,168
Composite layers	Hexahedral solid	112,500
Ceramic tiles	Hexahedral solid	1,350,000
UHMWPE	Hexahedral solid	562,500
Rigid clamps	Hexahedral solid	64,800
S-ALE mesh	Hexahedral solid	6,653,500

Table 1:   The type and the number of the elements in the numerical model of composite armor

Another analysis is modeled as the target being armor steel with the same area and weight as the ceramic composite armor. Similarly, this armor steel target is modeled with 248,842 three-dimensional solid hexahedral elements. This analysis can be modeled using axisymmetry to reduce the computational burden, thanks to the fact that there is no multi-layer composite part in the target. Thus, a quarter model is used, as seen in Fig. 3.
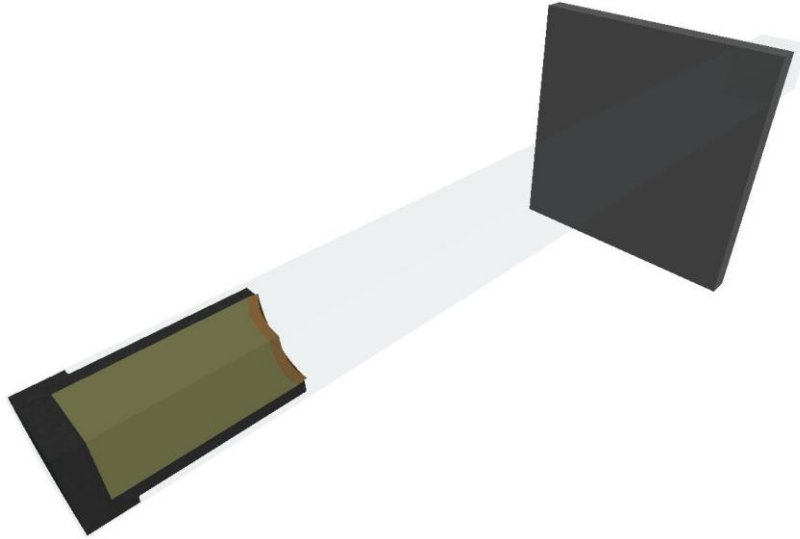
Fig.3: Axisymmetric ¼ model of EFP and armor steel together with S-ALE multi-material group domain

4.2   Materials

Table 2 represents the corresponding material models for each part and sources from the literature.

Part	Material Model	Source
Steel casing	MAT_015_Johnson_Cook	Johnson et al. [10]
High explosive	MAT_008_High_Explosive_Burn	Hu et al. [11]
OFHC copper liner	MAT_015_Johnson_Cook	Johnson et al. [10]
Composite	MAT_054_Enhanced_Composite_Damage	Bodepati et al. [12]
Ceramic tiles	MAT_110_Johnson_Holmquist_Ceramics	Cronin et al. [13]
UHMWPE	MAT_054_Enhanced_Composite_Damage	Xie et. al. [14]
Hardox400 Steel	MAT_107_Modified_Johnson_Cook	Børvik et al. [15]
Air	MAT_009 Null	Tabatabaei et. al. [16]

Table 2: Material models of the parts and their sources

Air, OHFC copper liner, high explosive S-ALE parts, and the steel casing require an equation of state (EoS) other than the constitutive model parameters. Table 3 shows the EoS models and sources.

Part	EoS Model	Source
Steel casing	Gruneisen	Hao [8]
High explosive	JWL	Hu et al. [11]
OFHC copper liner	Gruneisen	Hao [8]
Air	Linear Polynomial	Tabatabaei et. al. [16]

Table 3: Equation of state models of the parts and their sources

5   Results

The formation of the EFP slug and its shape during the roadside movement through the target is the first key result to obtain a good projectile before the impact. The shaping of the EFP, starting as a liner and becoming a slug, is represented in Fig. 4.
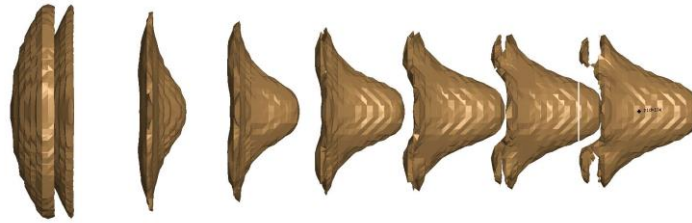
Fig.4: EFP slug formation from 0 to 70 µs with 10 µs increments

The main aim of the casing is to charge the high explosive material and to collimate the EFP slug through the desired direction. Fig. 5 represents the moment 50 µs after the explosion and the interaction between the high explosive, shaped liner, and the steel casing of the EFP. After 50 µs, the casing part is deleted from the analysis to reduce the computational burden by allowing the element erosion at that time.
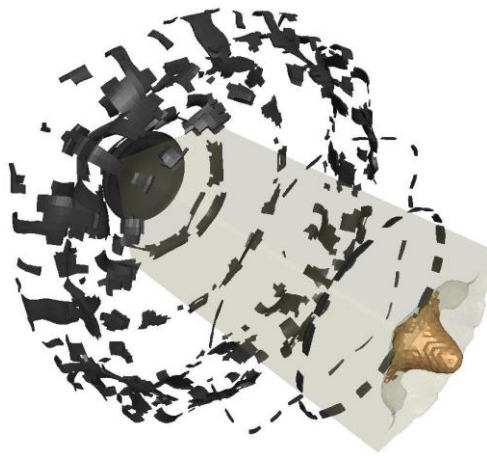
Fig.5: The state after 50 µs of casing, high explosive, and EFP slug

Just before the impact, the state between the ceramic composite armor and the EFP slug is shown in Fig. 6. Note that half of the composite panel elements are blanked in the following figures for simplicity. The EFP impact is just between the ceramic tiles, where a triple point between ceramics is formed due to the staggered tiling pattern. Since triple points cause ballistic vulnerabilities, it is aimed to push the limits of the ceramic composite armor.
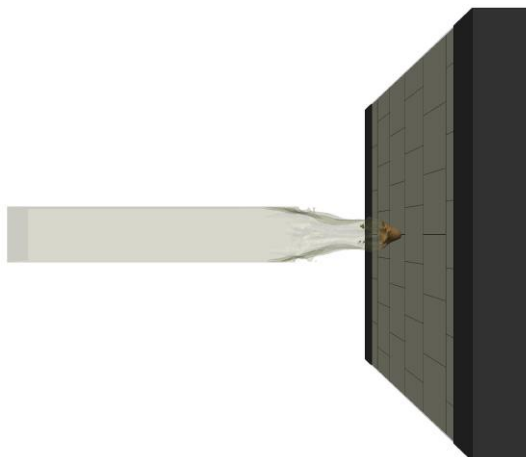
Fig.6: The state after 180 µs, just before the EFP impact on the ceramic composite armor

At the beginning of the impact, the hard ceramic tiles vigorously yield a large deformation on the copper EFP slug. Fig. 7 shows states between 190 and 210 µs.
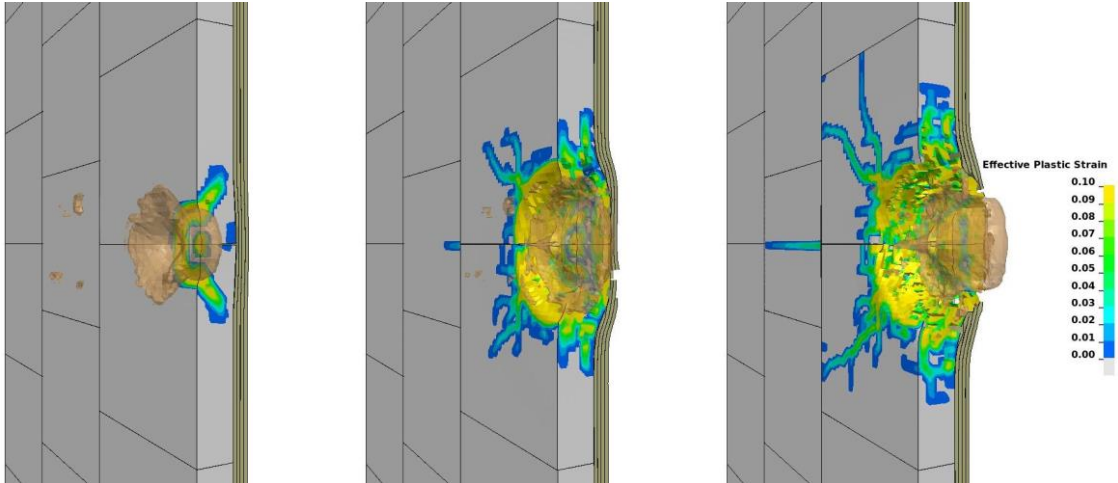
Fig.7:   FSI between the EFP slug and the composite armor with effective plastic strain contour bands on ceramic tiles at 190, 200, and 210 µs

At 210 µs, the EFP slug surpasses the ceramics and composite layer and encounters with UHMWPE. Fig. 8 represents the states between 220 and 400 µs.
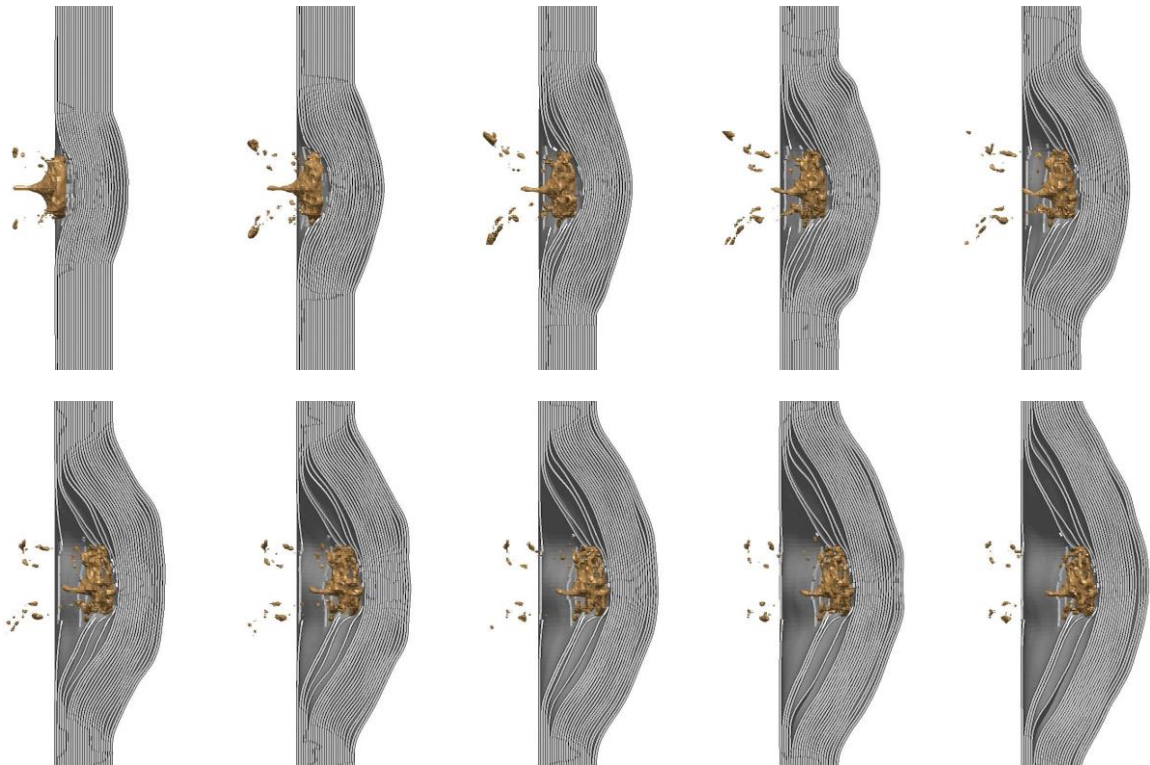
Fig.8:   FSI between the EFP slug and UHMWPE between 220-400 µs with 20 µs time increments

EFP slug is not a Lagrangian but a S-ALE part. Recall that energy balance controls are turned on during pre-processing. Also, rather than using history plots, "*matsum*" ASCII output is computed during the analysis to investigate the energies, velocities, displacements, etc., of the parts. Using this output, the rigid body velocity and the kinetic energy of the EFP slug S-ALE part are plotted in Fig. 9. It is observed that both the velocity and kinetic energy of the EFP slug vanishes at around 450 µs.
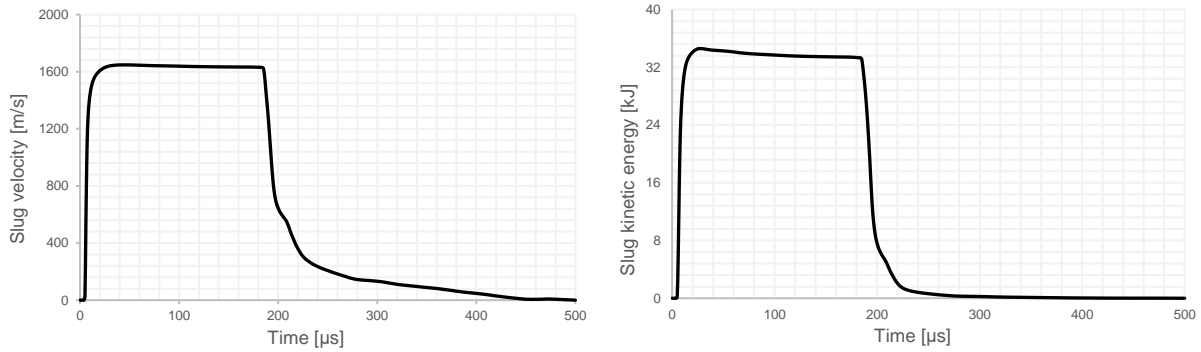
Fig.9: (a) Velocity and (b) kinetic energy histories of the EFP slug

Although the EFP impact on armor steel caused both the velocity and kinetic energy of the slug to vanish similarly, it also resulted in a complete penetration, as seen in Fig. 10. Furthermore, the impact region of the steel target became a shrapnel having a velocity more than 600 m/s, which might be a fatal threat to the surroundings.
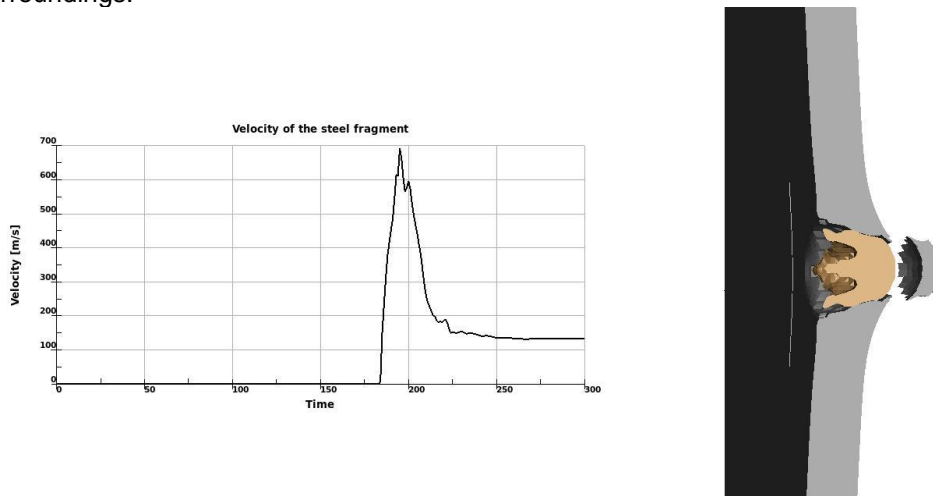
Fig.10: (a) Velocity vs. time diagram of the steel fragment and (b) the FSI between the EFP slug and the armor steel plate at 300 µs

As a result, from this study, one should deduce two main conclusions:
- At the same area and weight, ceramic composite armor provides much better ballistic protection than traditional steel armor,
- Ceramic composite armors can significantly reduce weight in armor solutions at the same ballistic protection level.

6   Summary

This research delved into assessing the ballistic capabilities of ceramic composite armors against EFP threats through numerical analysis employing LS-DYNA. The optimization and modeling of slug formation and its trajectory following impact were carried out using the S-ALE methodology, complemented by an enhanced fluid-structure interaction (FSI) algorithm. The investigation extensively examined the damage mechanics inflicted upon ceramic tiles, the behavior of polymeric components within the composite panel, and the EFP slug's resulting velocity and kinetic energy. A comparative analysis employing identical parameters of EFP threat was subsequently performed on a conventional armor steel target. This analysis facilitated a direct comparison between the ballistic performances of ceramic composite panels and armor steels. The findings indicate that ceramic composite armors exhibit significantly superior ballistic performance compared to ballistic steels of equivalent weight. Furthermore, they hold the potential to yield substantial advantages in terms of weight reduction.

7   Acknowledgements

8   Literature

[1]   J. J. Morrison, P. F. Mahoney, and T. Hodgetts, "Shaped charges and explosively formed penetrators: background for clinicians," *J R Army Med Corps*, vol. 153, no. 3, pp. 184–187, 2007, doi: 10.1136/JRAMC-153-03-11.

[2]   "Nurol Teknoloji." https://www.nurolteknoloji.com

[3]   J. O. Hallquist, "LS-DYNA ® Theory Manual," 2006.

[4]   C. Yu *et al.*, "Applied research of shaped charge technology," *Int J Impact Eng*, vol. 23, no. 1, pp. 981–988, Dec. 1999, doi: 10.1016/S0734-743X(99)00140-2.

[5]   C. Wang, T. Ma, and J. Ning, "Experimental investigation of penetration performance of shaped charge into concrete targets," *Acta Mechanica Sinica/Lixue Xuebao*, vol. 24, no. 3, pp. 345–349, Jun. 2008, doi: 10.1007/S10409-008-0160-3/METRICS.

[6]   D. Yang and J. Lin, "Numerical Investigation on the Formation and Penetration Behavior of Explosively Formed Projectile (EFP) with Variable Thickness Liner," *Symmetry 2021, Vol. 13, Page 1342*, vol. 13, no. 8, p. 1342, Jul. 2021, doi: 10.3390/SYM13081342.

[7]   L. Olovsson, "ALE and Fluid-Structure Interaction Capabilities in LS-DYNA."

[8]   "Introduction to Structured ALE | LSTC." https://ftp.lstc.com/anonymous/outgoing/hao/sale/

[9]   H. Chen, "On Setting up a Structured ALE Model."

[10]   G. R. Johnson and W. H. Cook, "Fracture characteristics of three metals subjected to various strains, strain rates, temperatures, and pressures," *Eng Fract Mech*, vol. 21, no. 1, pp. 31–48, Jan. 1985, doi 10.1016/0013-7944(85)90052-9.

[11]   F. Hu, H. Wu, Q. Fang, J. C. Liu, B. Liang, and X. Z. Kong, "Impact performance of explosively formed projectile (EFP) into concrete targets," *Int J Impact Eng*, vol. 109, pp. 150–166, Nov. 2017, doi: 10.1016/J.IJIMPENG.2017.06.010.

[12]   V. R. Bodepati, C. Jayarami Reddy, and M. Vemuri, "Numerical prediction of damage mechanisms of E-Glass/epoxy composite material against ballistic impact of 7.62 MS projectile," *https://doi.org/10.1177/2041419620967023*, vol. 12, no. 2, pp. 206–225, Nov. 2020, doi: 10.1177/2041419620967023.

[13]   D. S. Cronin, K. Bui, C. Kaufmann, G. Mcintosh, T. Berstad, and D. Cronin, "Implementation and Validation of the Johnson-Holmquist Ceramic Material Model in LS-Dyna."

[14]   Y. Xie, T. Wang, L. Wang, Y. Yang, and X. Sha, "Numerical investigation of ballistic performance of SiC/TC4/UHMWPE composite armor against 7.62 mm AP projectile," *Ceram Int*, vol. 48, no. 16, pp. 24079–24090, Aug. 2022, doi: 10.1016/J.CERAMINT.2022.05.088.

[15]   T. Børvik, S. Dey, and A. H. Clausen, "Perforation resistance of five different high-strength steel plates subjected to small-arms projectiles," *Int J Impact Eng*, vol. 36, no. 7, pp. 948–964, Jul. 2009, doi: 10.1016/J.IJIMPENG.2008.12.003.

[16]   Z. S. Tabatabaei and J. S. Volz, "2nd International LS-DYNA ® Users Conference A Comparison between Three Different Blast Methods in LS-DYNA ® : LBE, MM-ALE, Coupling of LBE and MM-ALE".